Anomaly Detection and Mode Identification in Multimode Processes using the Field Kalman Filter

Tian Cong, Ruomu Tan, James R. Ottewill, Nina F. Thornhill, *Senior Member, IEEE*, Jerzy Baranowski, *Member, IEEE*

***Abstract*—A process plant can have multiple modes of operation due to varying demand, availability of resources or the fundamental design of a process. Each of these modes is considered as normal operation. Anomalies in the process are characterised as deviations away from normal operation. Such anomalies can be indicative of developing faults which, if left unresolved, can lead to failures and unplanned downtime. The Field Kalman Filter (FKF) is a model-based approach, which is adopted in this paper for monitoring a multimode process. Previously, the FKF has been applied in process monitoring to differentiate normal operation from known faulty modes of operation. This paper extends the FKF so that it may detect occurrences of anomalies and differentiate them from the various normal modes of operation. A method is proposed for off-line training an FKF monitoring model and on-line monitoring. The off-line part comprises training an FKF model based on Multivariate Autoregressive State-Space (MARSS) models fitted to historical process data. A monitoring indicator is also introduced. On-line monitoring, on the basis of the FKF for anomaly detection and mode identification, is demonstrated using a simulated multimode process. The performance of the proposed method is also demonstrated using data obtained from a pilot-scale multiphase flow facility. The results show that the method can be applied successfully for anomaly detection and mode identification.**

***Index Terms*—Anomaly detection, Field Kalman Filter (FKF), Multivariate Autoregressive State-Space (MARSS) models, multimode process, mode identification**

I. Introduction

In process industries, the term *normal operation* refers to a plant running in a desired mode of operation. The fundamental goal of anomaly detection and mode identification is to differentiate various known operating modes, and to identify anomalies in a timely way to reduce or avoid downtime incidents. In order to enhance this monitoring performance, accurate mathematical models are required.

A linear time-invariant model in state-space form is a convenient approximation of a finite-order dynamic system in time-domain analysis (see e.g. [1]). Such models are able to describe the internal dynamics of a given physical process and its interaction with external inputs [2]. However, varying process demand causes a plant to operate in multiple operating modes. Single linear model approaches are inadequate for approximating processes with multiple operating modes due to the temporal relationships and correlations between variables for each operating mode being different from one another. Therefore, multiple linear models are required for monitoring a multimode process [3]. The efficiency and reliability of multiple model approaches for complex systems haven been investigated and discussed previously [4].

A bank of Kalman filters is a multi-model approach, rooted in the state-space formulation of a system with finite dimensional, usually discrete-time, linear dynamic subsystems. Its purpose is to recursively estimate the current states from the previous states and current measurements concurrently over multiple models. The residuals generated from a bank of Kalman filters can be used for classification, and have been used across a wide range of applications, such as differentiating various sensors and actuators in aircraft engines [5], [6], degrees of freedom of a quad rotor [7], detecting fading channels in mobile communications [8] and mechanical failure and sensor failure [9]. Further evaluation of the residuals combined with Bayes' theorem leads to a model-based statistical decision approach which may be used, for example, for fault diagnosis [10], [11].

The Field Kalman Filter (FKF) is a model-based approach in which a system is described in a continuous-parameter-dependent state-space form. It is a Bayesian algorithm, which allows simultaneous estimation of the state, system parameters and noise parameters [12]. In case of continuously distributed system and noise parameters, FKF, while inherently infinite dimensional, can be efficiently approximated using an appropriately selected bank of Kalman filters and a Bayesian updating scheme for reconstructing the joint posterior of state and parameters. If parameters have discrete distributions no approximation is needed, as a bank of Kalman filters is created naturally while the posterior distribution is also reconstructed properly.

The FKF holds a range of advantages related to other, comparable approaches. Firstly, the FKF is able to handle systems with unknown noise characteristics (but with known distribution of their parameters). As a result, the operating modes can be differentiated not only deterministically but also stochastically. Secondly, the probabilistic monitoring results are traceable and interpretable for operators. Finally, because forgetting factors are incorporated into its formulation, the FKF can continue to operate reliably even when the parameters of the system change.

Manuscript created October 01, 2019; revised ,2019. This work was supported by the European Union's Horizon 2020 research and innovation programme under grant agreement No. 675215 - PRONTO - H2020-MSCA-ITN-2015.

T. Cong and J. Baranowski are with the Department of Automatic Control and Robotics, AGH University of Science and Technology, Kraków, Poland (e-mail: cong@agh.edu.pl, jb@agh.edu.pl).

R. Tan and N.F. Thornhill are with the Centre for Process Systems Engineering, Imperial College London, London, U.K. (e-mail: r.tan@imperial.ac.uk, n.thornhill@imperial.ac.uk).

J.R. Ottewill is with Hitachi ABB Power Grids Research, Kraków, Poland (e-mail: james.ottewill@hitachi-powergrids.com).

In previous work [13], FKF was used for analysis of problems where a discrete character of parameter distribution came from the distinction of healthy/faulty operation. In that approach, models of all possible parameter realisations had to be known. In this paper, we extend FKF to allow not only mode identification in a multimode process but also detection of unknown modes.

In process monitoring applications, it is often challenging to accurately model a process. One popular working direction within the process industries is to use historical data to build data-driven process models. The FKF requires models to be provided in a state-space form. There are many data-based approaches for obtaining the state-space formulation, such as Gaussian regression [14], [15] and Canonical Variate Analysis [16]. In this paper, the Multivariate Autoregressive State-Space approach (MARSS) [17] is adopted. Autoregressive (AR) models have been used for modelling a steady-state process [18]. An AR model may be converted to a state-space form [17].

Data obtained during periods of faulty operation are often nonlinear in nature [19]. Models obtained using these data may be inaccurate because simplifying assumptions have to be made in order to provide a tractable solution [20]. In addition, faults are rare occurrences and there may not be any historical data for fault conditions. Conversely, sufficient data from normal operation are often available from industrial plants. Furthermore, the local dynamics in the normal process may be well captured by a linear discrete model.

When applied to process monitoring, Bayesian methods for classification are limited to known process models. Therefore, the methods are unable to detect the occurrence of faults or new operating modes. To address this problem, Song et al. [21] proposed to build several statistical models corresponding to normal operating modes and several monitoring indicators for detecting anomalies. The monitoring structure is to perform Bayes' statistical decision-based classification and to detect anomalies relying on its monitoring indicator. In addition, other research efforts focus on strategies of integrating the Bayes' statistical decisions for detecting anomalies in a process with multiple operating modes [19], [22].

The statistical decisions in Bayes' theorem refer to posterior probabilities. In practice, there may be a numerical problem when the numerator and the denominator in the fraction for calculating the posterior probability are extremely small values [13]. In Bayes' theorem, the denominator is the sum of products of the likelihood probability and prior probability. An extremely small denominator can indicate the occurrence of anomalies and is the same across all the known operating modes. A unified monitoring indicator for anomaly detection in the FKF framework can be designed. The detection of anomalies removes the necessity of mode identification, thereby sidestepping the calculation of posterior probabilities, thus the numerical problem caused by the anomalies can be avoided.

The main contributions of this paper are as follows:

- The FKF is applied for monitoring multimode processes including anomaly detection and mode identification;
- A method comprising off-line training of an FKF monitoring model and on-line monitoring is proposed. The off-line training of an FKF monitoring model includes the derivation of the FKF model and a unified monitoring indicator. The FKF model is trained with MARSS models incorporating historical data. A unified monitoring indicator extends the FKF so that it may also used for anomaly detection applications;
- The performance of the FKF monitoring model is demonstrated in a simulated multimode process consisting of three models, having the following behaviours:
  1) same steady-state, with three different dynamics,
  2) three different steady-states with the same dynamics,
  3) three different steady-states and three different dynamics;
- The proposed method is validated on data obtained from a pilot-scale multiphase flow facility [23] with multiple operating modes and a fault.

The rest of paper is organised as follows: Section II introduces the identification of MARSS models incorporating historical data, the theoretical formulation of FKF, and the use of FKF for anomaly detection and mode identification. The procedure of off-line training an FKF monitoring model and on-line monitoring is given in Section III. Section IV evaluates the training of the FKF model using a simulated multimode process. Section V validates the proposed method on data recorded from an industrial scale multiphase flow facility. Also in Section V, a comparison study is conducted with other process monitoring methods. The paper ends with conclusions.

II. Methodology

A. Preliminary

1) Field Kalman Filter (FKF): A parameter-dependent state-space model is defined as:

$$\begin{aligned} \boldsymbol{x}[t+1] &= A(\theta)\boldsymbol{x}[t] + B(\theta)\boldsymbol{u}[t] + \boldsymbol{w}[t] \\ \boldsymbol{y}[t] &= C(\theta)\boldsymbol{x}[t] + \boldsymbol{v}[t] \\ \boldsymbol{w}[t] &\sim \mathcal{N}(0, W(\theta)), \boldsymbol{v}[t] \sim \mathcal{N}(0, V(\theta)) \end{aligned} \tag{1}$$

where $\boldsymbol{x}[t] \in \mathbb{R}^m$ is the state, $\boldsymbol{y}[t] \in \mathbb{R}^r$ is the measurement, $\boldsymbol{w}[t] \in \mathbb{R}^m$ is the state noise, $\boldsymbol{v}[t] \in \mathbb{R}^r$ is the measurement noise, $\boldsymbol{u}[t] \in \mathbb{R}^l$ is the system input, $\theta \in \Omega \subset \mathbb{R}^p$ is a vector of parameters and $\mathcal{N}$ represents the Gaussian distribution. m is the number of state variables and r is the number of measurement variables. The matrix functions A, B, C, W, V are of C^1 class [1] w.r.t. θ. $A(\theta)$, $B(\theta)$, $C(\theta)$, $W(\theta)$ and $V(\theta)$ respectively denote the state transition matrix, input-control matrix, measurement-control matrix, state noise covariance and measurement noise covariance, and are of appropriate dimensions.

Let $\boldsymbol{y}_t = \boldsymbol{y}[t]$ and $\boldsymbol{x}_t = \boldsymbol{x}[t]$. Considering a sequence of measurements $\boldsymbol{y}_1, \boldsymbol{y}_2, \ldots$ and corresponding states $\boldsymbol{x}_1, \boldsymbol{x}_2, \ldots$, the main objective of the FKF is to simultaneously

[1] C^1 class refers to all of the differentiable functions whose derivative is continuous.

estimate the distribution of state $\boldsymbol{x}_t$ and parameter θ, $P(\boldsymbol{x}_t, \theta)$. The past measurements for the time interval $(0, t-1]$ can be written as

$$Y_{t-1} = \begin{cases} \{\boldsymbol{y}_1, \ldots, \boldsymbol{y}_{t-1}\}, & \text{for } t = 2, 3, \ldots \\ \varnothing, & \text{for } t = 1. \end{cases} \tag{2}$$

The FKF estimates $P(\boldsymbol{x}_t, \theta)$ in a recursive manner incorporating the information of past measurements Y_{t-1} as well as the current measurement $\boldsymbol{y}_t$. There are two main steps for each iteration in the recursive process summarised as:

- Prediction of joint distribution $P(\boldsymbol{x}_t, \theta | Y_{t-1})$;
- Correction of joint distribution $P(\boldsymbol{x}_t, \theta | Y_{t-1}, \boldsymbol{y}_t) = P(\boldsymbol{x}_t, \theta | Y_t)$.

Assuming $\Omega = \{\theta_j, j = 1, \ldots, J\}$ converts model (1) into a set of θ_j-dependent state-space models, resulting in a structure similar to other multiple model approaches. As these θ_j-dependent state-space models are obtained from the FKF, they are referred to as the FKF model. Under the assumption of $P(\theta_1|Y_t) \neq \cdots \neq P(\theta_J|Y_t)$, $P(\boldsymbol{x}_t, \theta|Y_{t-1})$ and $P(\boldsymbol{x}_t, \theta|Y_t)$ both are probability mass functions for the variable θ that can take J discrete values, which is the key property of the FKF being utilised for anomaly detection and mode identification.

In the application of monitoring a process with J operating modes, parameters in (1) are drawn from sets with J members. The FKF model does not require the explicit values of $\theta_1, \ldots, \theta_J$, instead only the matrix functions of θ_j are of interest, which are expressed as $\forall j$, $A(\theta) = \{A(\theta_j)\}$, $B(\theta) = \{B(\theta_j)\}$, $C(\theta) = \{C(\theta_j)\}$, $W(\theta) = \{W(\theta_j)\}$ and $V(\theta) = \{V(\theta_j)\}$. This paper also considers the case when $j \notin \{1, \ldots, J\}$, related to the appearance of anomalies.

2) Data preparation: Historical data-based approaches for monitoring multimode processes typically begin with a data partitioning step [24]. Data recorded from various operating modes can be partitioned manually by experts, and outliers existing in the historical data can be discarded using appropriate techniques [25]. Given healthy data, the partition can also be automated by clustering algorithms, for example, Dirichlet Process (DP) [26]. The DP is able to cluster the data automatically with respect to operating modes without knowing the number of modes in advance, leading to a reasonable value of J. As a result, historical data Y_{H} are partitioned according to operating modes as $Y_{\text{H}} = \{Y_{\text{H}}^{(j)}, j = 1, 2, \ldots, J\}$ where J is the number of operating modes and $Y_{\text{H}}^{(j)}$ denotes the historical data for the j-th operating mode. For the j-th operating mode, historical data $Y_{\text{H}}^{(j)}$ are further split into a training dataset $Y_{\text{Tr}}^{(j)}$ and a validation dataset $Y_{\text{Va}}^{(j)}$.

B. Multivariate Autoregressive State-Space (MARSS) models

The acquisition of the state-space models of normal operating modes is conducted using historical process data.

1) Multivariate Autoregressive (MAR) models: In this paper, the r-dimension MAR model having k autoregressive terms and a constant term takes the form

$$\boldsymbol{y}^{(j)}[t+1] = \Phi_1^{(j)} \boldsymbol{y}^{(j)}[t] + \cdots + \Phi_k^{(j)} \boldsymbol{y}^{(j)}[t-k+1] + \Phi_0^{(j)} \tag{3}$$

where $\boldsymbol{y}^{(j)}[t+1], \boldsymbol{y}^{(j)}[t], \ldots, \boldsymbol{y}^{(j)}[t-k+1] \in \mathbb{R}^r$ represents variable vectors equally spaced in time, $\Phi_1^{(j)}, \ldots, \Phi_k^{(j)} \in \mathbb{R}^{r \times r}$ are coefficient matrices, and $\Phi_0^{(j)} \in \mathbb{R}^r$ is a coefficient vector for the j-th mode.

Using a least squares fitting procedure [27], the coefficients $\Phi_1^{(j)}, \ldots, \Phi_k^{(j)}, \Phi_0^{(j)}$ can be obtained by fitting the model in (3) to an ensemble of measurements $Y_{\text{H}}^{(j)}$ [28].

2) Conversion of an MAR model to state-space form: When $\Omega = \{\theta_j, j = 1, \ldots, J\}$, the desired state-space form is

$$\begin{aligned} \boldsymbol{x}(\theta_j)[t+1] &= \hat{A}(\theta_j)\boldsymbol{x}(\theta_j)[t] + \hat{B}(\theta_j)\boldsymbol{u}[t] + \boldsymbol{w}(\theta_j)[t] \\ \boldsymbol{y}(\theta_j)[t] &= \hat{C}(\theta_j)\boldsymbol{x}(\theta_j)[t] + \boldsymbol{v}(\theta_j)[t] \\ \boldsymbol{w}(\theta_j)[t] &\sim \mathcal{N}(0, \hat{W}(\theta_j)), \boldsymbol{v}(\theta_j)[t] \sim \mathcal{N}(0, \hat{V}(\theta_j)) \\ & j = 1, \ldots, J \end{aligned} \tag{4}$$

where $\hat{A}(\theta_j)$, $\hat{B}(\theta_j)$, $\hat{C}(\theta_j)$, $\hat{W}(\theta_j)$ and $\hat{V}(\theta_j)$ are the estimates of state transition matrix, input-control matrix and measurement-control matrix, state noise covariance and measurement noise covariance of the j-th mode, respectively. $\boldsymbol{w}(\theta_j)[t]$ and $\boldsymbol{v}(\theta_j)[t]$ are samples from zero-mean Gaussian distributions with noise covariances $\hat{W}(\theta_j)$ and $\hat{V}(\theta_j)$, respectively. $\boldsymbol{x}(\theta_j)[t]$ and $\boldsymbol{y}(\theta_j)[t]$ are the calculated state and measurement using (4). The variable $\boldsymbol{u}[t]$ is equal to 1, because there is a constant term in (3).

As (3) is to be converted to a state-space model, it is necessary to choose some states. There are many possible choices for the states [17]. In this paper the states are given by

$$\boldsymbol{x}(\theta_j)[t] = \begin{pmatrix} \boldsymbol{x}_1[t] \\ \boldsymbol{x}_2[t] \\ \vdots \\ \boldsymbol{x}_k[t] \end{pmatrix} \tag{5}$$

where

$$\boldsymbol{x}_i[t] = \begin{cases} \boldsymbol{y}^{(j)}[t] \in \mathbb{R}^r, & \text{for } i = 1 \\ \boldsymbol{x}_1[t-i+1] \in \mathbb{R}^r, & \text{for } i = 2, 3, \ldots, k. \end{cases} \tag{6}$$

With these definitions, $\hat{A}(\theta_j), \hat{B}(\theta_j)$ and $\hat{C}(\theta_j)$ in (4) can be given as:

$$\begin{aligned} \hat{A}(\theta_j) &= \left(\begin{array}{c|c|c|c} \Phi_1^{(j)} & \Phi_2^{(j)} & \ldots & \Phi_k^{(j)} \\ \hline \boldsymbol{I} & \boldsymbol{0} & \ldots & \boldsymbol{0} \\ \hline \vdots & \vdots & \ddots & \vdots \\ \hline \boldsymbol{0} & \ldots & \boldsymbol{I} & \boldsymbol{0} \end{array}\right) \in \mathbb{R}^{rk \times rk} \\ \hat{B}(\theta_j) &= \left(\begin{array}{c} \Phi_0^{(j)} \\ \hline 0 \\ \hline \vdots \\ \hline 0 \end{array}\right) \in \mathbb{R}^{rk} \\ \hat{C}(\theta_j) &= \left(\begin{array}{c|c|c|c} \boldsymbol{I} & \boldsymbol{0} & \ldots & \boldsymbol{0} \end{array}\right) \in \mathbb{R}^{r \times rk}, \end{aligned} \tag{7}$$

where the dotted lines indicate that the vectors and matrices have sub-blocks, $\boldsymbol{I} \in \mathbb{R}^{r \times r}$ is an identity matrix and $\boldsymbol{0} \in \mathbb{R}^{r \times r}$ is a matrix with all elements of value 0.

The noises $\boldsymbol{w}(\theta_j)[t]$ and $\boldsymbol{v}(\theta_j)[t]$ for states and outputs are assumed subject to zero mean, uncorrelated Gaussian distributions. Thus, covariance matrices $\hat{W}(\theta_j)$ and $\hat{V}(\theta_j)$ are diagonal matrices, being estimated using validation dataset $Y_{\text{Va}} = \{Y_{\text{Va}}^{(1)}, \ldots, Y_{\text{Va}}^{(J)}\}$.

C. FKF for monitoring a multimode process

When $\Omega = \{\theta_1, \ldots, \theta_J\}$, the FKF model for a J-mode process can be formulated as (4). Generally, the parameter matrices in (4) are unknown. The FKF model can be trained by the method in Section II-B. The FKF algorithm supporting $\theta \in \{\theta_1, \ldots, \theta_J\}$ is presented in Fig. 1.

The recursive process in FKF includes two main steps:

1) Prediction step. The prediction step determines the joint probability distribution of $\boldsymbol{x}_t$ and θ using past measurements Y_{t-1}:

$$P(\boldsymbol{x}_t, \theta | Y_{t-1}) = P(\boldsymbol{x}_t | \theta, Y_{t-1}) P(\theta | Y_{t-1}) \tag{8}$$

where $P(\boldsymbol{x}_t|\theta, Y_{t-1})$ follows a mixture of Gaussian distributions. Each Gaussian component is predicted in the same way as in a Kalman filter, having a mean vector $\boldsymbol{x}_t^-(\theta_j)$ as equation (17a) in Fig. 1 and a covariance $S_t^-(\theta_j)$ as (17b) in Fig. 1. $P(\theta|Y_{t-1})$ is the distribution of Gaussian components. At $t = 1$, $P(\theta|Y_{t-1}) = P_0^+(\theta)$ is presumed uniformly distributed as (16e).

2) Correction step. The correction step determines the joint probability distribution of $\boldsymbol{x}_t, \theta$ with additional measurement $\boldsymbol{y}_t$:

$$\begin{aligned} P(\boldsymbol{x}_t, \theta | Y_{t-1}, \boldsymbol{y}_t) &= P(\boldsymbol{x}_t | \theta, Y_{t-1}, \boldsymbol{y}_t) P(\theta | Y_{t-1}, \boldsymbol{y}_t) \\ &= P(\boldsymbol{x}_t | \theta, Y_{t-1}, \boldsymbol{y}_t) \\ &\quad \times P(\boldsymbol{y}_t | \theta, Y_{t-1}) P(\theta | Y_{t-1}) \end{aligned} \tag{9}$$

where $P(\boldsymbol{x}_t|\theta, Y_{t-1}, \boldsymbol{y}_t)$ follows a mixture of corrected Gaussian distributions where each Gaussian component is parameterised by mean vector $\boldsymbol{x}_t^+(\theta_j)$ as (18b) and covariance $S_t^+(\theta_j)$ as (18c). At $t = 1$, since $Y_{t-1} = \varnothing$, often $P(\boldsymbol{x}_t|\theta, Y_{t-1}, \boldsymbol{y}_t) = P(\boldsymbol{x}_t|\theta, \boldsymbol{y}_t)$ in which case the $\boldsymbol{x}_{t-1}^+(\theta_j) = \boldsymbol{x}_0^+(\theta_j)$ in (17a) is initialised as a zero vector and $S_{t-1}^+(\theta_j) = S_0^+(\theta_j)$ in (17b) is an identity matrix. $P(\boldsymbol{y}_t|\theta, Y_{t-1})$ can be estimated by $P(\boldsymbol{x}_t|\theta, Y_{t-1}, \boldsymbol{y}_t)$ because $\boldsymbol{y}_t$ is linearly linked to $\boldsymbol{x}_t$ and both noise covariances of $\boldsymbol{x}_t$ and $\boldsymbol{y}_t$ are Gaussian. Therefore, $P(\boldsymbol{y}_t|\theta, Y_{t-1})$ is also a mixture of Gaussian distributions with mean vector $\boldsymbol{y}_t^-(\theta_j)$ as (18d) and covariance $\boldsymbol{M}_t^-(\theta_j)$ as (18e) for the j-th component.

Since $\theta \in \{\theta_1, \ldots, \theta_J\}$, each time instant yields J conditional probabilities with respect to $\boldsymbol{x}_t$ and θ. As a plant may run at only one operating mode at a time, only one conditional probability is the best-fit to reflect the current operation. The inference of the best-fit conditional probability is equivalent to finding the θ_j at time t to give the best estimates of measurement $\boldsymbol{y}_t$. It should be noted that actual dependence of the MARSS model on parameters θ is strongly implicit. In the considered case, it is not necessary to explicitly estimate parameters, as the interest is in the mode classification and anomaly detection.

Let $I_t \in \{1, \ldots, J\}$ be the mode identity at time t. $I_t = j$ implies that all the past measures $\boldsymbol{y}_{t-1}, \boldsymbol{y}_{t-2}, \ldots, \boldsymbol{y}_1$ were from the j-th mode associated with system information $A(\theta_j), B(\theta_j), C(\theta_j), W(\theta_j), V(\theta_j)$. The posterior probability of a plant running at the j-th mode given $\boldsymbol{y}_t$ can be formulated according to Bayes' theorem:

$$\begin{aligned} P(\boldsymbol{y}_{t-1}, \boldsymbol{y}_{t-2}, \ldots, \boldsymbol{y}_1, &A(\theta_j), B(\theta_j), C(\theta_j), W(\theta_j), V(\theta_j) | \boldsymbol{y}_t) \\ &= P(I_t = j | \boldsymbol{y}_t) \\ &= \frac{P(\boldsymbol{y}_t | I_t = j) P(I_t = j)}{\sum_{j=1}^{J} P(\boldsymbol{y}_t | I_t = j) P(I_t = j)} \end{aligned} \tag{10}$$

where $P(I_t = j)$ is the prior probability of a plant running at the j-th mode before $\boldsymbol{y}_t$ is measured, $P(\boldsymbol{y}_t|I_t = j)$ is the likelihood probability of measuring $\boldsymbol{y}_t$ when a plant is running at the j-th mode and $P(I_t = j \mid \boldsymbol{y}_t)$ is the posterior probability of a plant running at the j-th mode given $\boldsymbol{y}_t$.

Under the assumption of Gaussian distribution, the likelihood probability can be calculated by

$$\begin{aligned} P(\boldsymbol{y}_t | I_t = j) &= P(\boldsymbol{y}_t | \boldsymbol{y}_t \sim \mathcal{N}(\boldsymbol{y}_t^-(\theta_j), \boldsymbol{M}_t^-(\theta_j))) \\ &= \det(2\pi \boldsymbol{M}_t^-(\theta_j))^{-\frac{1}{2}} \\ &\quad \times \exp^{-\frac{1}{2}(\boldsymbol{y}_t - \boldsymbol{y}_t^-(\theta_j))^\top (\boldsymbol{M}_t^-(\theta_j))^{-1} (\boldsymbol{y}_t - \boldsymbol{y}_t^-(\theta_j))}. \end{aligned} \tag{11}$$

In this paper, there is no prior assumption regarding the probabilities between operating modes. The common way of assigning $P(I_t = j)$ is recursive. Before having any measurements, the prior probability $P(I_t = j)$ for $j = 1, \ldots, J$ are set equal to $\frac{1}{J}$ due to lack of prior knowledge. Once measurements arrive, the prior probability $P(I_t = j)$ is updated with the posterior probability $P(I_{t-1} = j|\boldsymbol{y}_{t-1})$. However, the drawback of this simple posterior-to-prior updating is that if any prior is updated with its posterior of value 0 (or numerically indistinguishable from it), both prior and posterior values will be locked to 0 for further computation. This can be problematic in cases of mode switching. In similar approaches [10], [11], [29], prior probabilities are artificially lower bounded by a small value, which is a design parameter. In the case of FKF, to overcome this issue the prior distributions are updated using the forgetting operator [13]:

$$F(\alpha) = \frac{1}{2} \begin{pmatrix} 1+\alpha & 1-\alpha & & & & & \\ 1-\alpha & 2\alpha & 1-\alpha & & & & \\ & 1-\alpha & 2\alpha & 1-\alpha & & & \\ & & \ddots & \ddots & \ddots & & \\ & & & 1-\alpha & 2\alpha & 1-\alpha & \\ & & & & 1-\alpha & 1+\alpha \end{pmatrix} \tag{12}$$

where $F(\alpha) \in \mathbb{R}^{J \times J}$, $\alpha \in (0, 1)$ is a forgetting factor and the unfilled entries are zeros. The use of forgetting factor still guarantees that the sum of priors is 1. Then instead of directly taking over the posterior values, the prior values are predicted by (17c) in Fig. 1 where

$$P_t^-(\theta) = \begin{pmatrix} P(I_t = 1) \\ P(I_t = 2) \\ \vdots \\ P(I_t = J) \end{pmatrix} \tag{13}$$

$$P_{t-1}^{+}(\theta) = \begin{pmatrix} P(I_{t-1}=1|\boldsymbol{y}_{t-1}) \\ P(I_{t-1}=2|\boldsymbol{y}_{t-1}) \\ \vdots \\ P(I_{t-1}=J|\boldsymbol{y}_{t-1}) \end{pmatrix}. \tag{14}$$

If the forgetting factor α is set close to its upper bound value 1, it means that the prior values of time t are updated with the posterior values of time $t-1$. If α is close to 0, the prior probability of time t is no longer influenced by its posterior probability at time $t-1$, and instead is predicted using the sum of other weighted posterior probabilities at time $t-1$. The reason is that the stationary distribution for $F(\alpha)$ is uniform:

$$\lim_{t\to\infty} F(\alpha)^t P_0 = (\frac{1}{J}, \frac{1}{J}, \ldots, \frac{1}{J})^\top \in \mathbb{R}^J \quad \text{for any } P_0 \in \mathbb{R}^J. \tag{15}$$

In practice, α can be adjusted according to specific applications. Here, we set $\alpha = 0.99$.

D. Anomaly detection and mode identification

Bayes' theorem has limitations when measurements have large variance [13], or when the measurements are from a mode $j \notin \{1, \ldots, J\}$ (e.g. new operating modes or faults) [19], [22]. The likelihoods of the measurements given $j \notin \{1, \ldots, J\}$ will be close to 0, leading to a numerical problem in calculating the posterior probability because the denominator in (10) will be close to 0. Bayes' theorem can still be applied to anomaly detection by utilising a small value as the monitoring threshold.

This paper proposes a monitoring indicator L_t

$$L_t = \sum_{j=1}^{J} P(\boldsymbol{y}_t | I_t = j). \tag{19}$$

An anomaly is detected when the following condition holds for L_t:

$$L_t < L_{\text{LML}}. \tag{20}$$

where L_{LML} is the lower monitoring limit estimated from the validation data $Y_{\text{Va}} = \{Y_{\text{Va}}^{(1)}, \ldots, Y_{\text{Va}}^{(J)}\}$. L_{LML} is set with the fifth percentile of the values of L_t. These monitoring indicators are obtained by feeding Y_{Va} to the Algorithm 1 in which the calculation of the predicted and corrected prior probabilities in (17c), (18f) and (18g) are skipped and L_t is calculated by (19). The usage of validation data here is to simulate the on-line data of normal operation. The L_{LML} is a cutoff point in the validation data for flagging anomalies.

The mode identity at time t is determined by:

$$\arg\max_j P(I_t = j | \boldsymbol{y}_t). \tag{21}$$

Fig. 2 presents the workflow of anomaly detection and mode identification based on the FKF. Given the FKF model and L_{LML}, the monitoring indicator at time t for the measurement $\boldsymbol{y}_t$ is calculated using (19). If $L_t < L_{\text{LML}}$, $I_t \notin \{1, \ldots, J\}$ denotes that $\boldsymbol{y}_t$ is an anomaly. There is no need to conduct mode identification. Hence, let $P_t^+(\theta_j) = 0 \ \forall j$ as (22a) be indicative of the appearance of an anomaly. The predicted prior distribution of all the known operating modes for the next time instant are set to a uniform distribution as (22b). If $\boldsymbol{y}_t$ is recognised as normal operation, the mode identity is determined by (21).

Algorithm 1: Field Kalman Filter (FKF)

Initialisation

$$\theta \in \{\theta_1, \ldots, \theta_J\} \tag{16a}$$
$$t = 1, \forall j = 1, \ldots, J \tag{16b}$$
$$\boldsymbol{x}_0^+(\theta_j),\ S_0^+(\theta_j) \tag{16c}$$
$$P_0^+(\theta_1) = \ldots, P_0^+(\theta_J) = \frac{1}{J} \tag{16d}$$
$$P_0^+(\theta) = (P_0^+(\theta_1), \ldots, P_0^+(\theta_J))^\top \tag{16e}$$

Prediction step

Predicted state:
$$\boldsymbol{x}_t^-(\theta_j) = A(\theta_j)\boldsymbol{x}_{t-1}^+(\theta_j) + B(\theta_j)\boldsymbol{u}[t] \tag{17a}$$
Predicted noise covariance of state:
$$S_t^-(\theta_j) = A(\theta_j)S_{t-1}^+(\theta_j)A(\theta_j)^\top + W(\theta_j) \tag{17b}$$
Predicted prior distribution of $I_t = 1, \ldots, I_t = J$:
$$P_t^-(\theta) = F(\alpha)P_{t-1}^+(\theta) \tag{17c}$$

Correction step

Kalman gain:
$$K_t(\theta_j) = S_t^-(\theta_j)C(\theta_j)^\top M_t^-(\theta_j)^{-1} \tag{18a}$$
Corrected state:
$$\boldsymbol{x}_t^+(\theta_j) = K_t(\theta_j)(\boldsymbol{y}_t - \boldsymbol{y}_t^-(\theta_j)) + \boldsymbol{x}_t^-(\theta_j) \tag{18b}$$
Corrected noise covariance of state:
$$S_t^+(\theta_j) = (\boldsymbol{I} - K_t(\theta_j)C(\theta_j))S_t^-(\theta_j) \times (\boldsymbol{I} - K_t(\theta_j)C(\theta_j))^\top + K_t(\theta_j)V(\theta_j)K_t(\theta_j)^\top \tag{18c}$$
Predicted measurement:
$$\boldsymbol{y}_t^-(\theta_j) = C(\theta_j)\boldsymbol{x}_t^-(\theta_j) \tag{18d}$$
Predicted noise covariance of measurement:
$$M_t^-(\theta_j) = V(\theta_j) + C(\theta_j)S_t^-(\theta_j)C(\theta_j)^\top \tag{18e}$$
Posterior probability of $I_t = j$:
$$P_t^+(\theta_j) = P(I_t = j|\boldsymbol{y}_t) = \frac{P(\boldsymbol{y}_t|I_t = j)P_t^-(I_t = j)}{\sum_{j=1}^{J} P(\boldsymbol{y}_t|I_t = j)P_t^-(I_t = j)} \tag{18f}$$
Posterior distribution of $I_t = 1, \ldots, I_t = J$:
$$P_t^+(\theta) = (P_t^+(\theta_1), \ldots, P_t^+(\theta_J))^\top \tag{18g}$$
$$t = t + 1 \tag{18h}$$

Go to prediction step until process stops

Fig. 1. The algorithm of the FKF when $\theta \in \{\theta_1, \ldots, \theta_J\}$. The superscript $^+$ denotes the corrected variable and $^-$ denotes the predicted variable.

III. Workflow for Anomaly Detection and Mode Identification

The proposed workflow in Fig. 3 illustrates how to practically apply the FKF for monitoring multimode processes. The left side of Fig. 3 shows the off-line training of the FKF monitoring model, including the acquisition of the FKF model and the determination of an L_{LML}. Training the FKF model entails MARSS learning using training data and noise estimation using validation data. During on-line monitoring,

Algorithm 2: Anomaly detection and mode identification

The FKF model as (4) is trained according to the Section II-B.
The lower monitoring limit L_{LML} is derived according to the Section II-D.
Time stamp t is initialised to 1.
while *Process continues* **do**
  $L_t = \sum_{j=1}^{J} P(\boldsymbol{y}_t | I_t = j)$
  if $L_t < L_{LML}$ **then**
    $\boldsymbol{y}_t$ is an anomaly, indicating $I_t \notin \{1, \ldots, J\}$.
    Instead of (17c) and (18f), the predicted and corrected prior probabilities are calculated using the following equations:

$$P_t^+(\theta_j) = P(I_t = j | \boldsymbol{y}_t) = 0 \quad \forall j \tag{22a}$$

$$P_{t+1}^-(\theta_j) = P(I_{t+1} = j) = \frac{1}{J} \quad \forall j. \tag{22b}$$

  else
    $\boldsymbol{y}_t$ is recognised as normal operation.
    $\forall j = 1, \ldots, J$, the predicted and corrected prior probabilities are calculated using (17c), (18f) and (18g).
    The mode identify I_t is determined by (21).
    $t = t + 1$
  end
end

Fig. 2. On-line monitoring with the FKF monitoring model

a new incoming measurement $\boldsymbol{y}_t$ is checked for normal or anomalous operation using L_{LML}. If $\boldsymbol{y}_t$ is recognised as normal operation, it will be classified to one of the known operating modes. The prior distribution of known operating modes is updated according to Algorithm 2 so that it may be used for anomaly detection and mode identification of the next data sample.

IV. Simulated case study

A. Dynamic and steady-state models

The simulation example investigates the performance of the FKF algorithm with data from a simulated multimode process. Output data from the process are derived from three multimode simulation models that have the following behaviours: 1) same steady-state with three different dynamics, 2) three different steady-states with the same dynamics and 3) three different steady-states and three different dynamics. Fig. 4 shows the step responses of the models as dashed-lines. Parameter specifications of these models are shown in the Appendix.

These models were defined to give a range of under-damped and over-damped transient dynamics, as shown in Fig. 4. Applied with unit step inputs and uncorrelated, white Gaussian noise $\mathcal{N}(0, 0.1)$, starting at zero initial conditions, all of the state-space models were run separately to obtain training and validation data. Data of both transient response and fluctuations around steady-states were included in training and validation datasets. The test data were generated by running one of the simulation models with a unit step, noise $\mathcal{N}(0, 0.1)$ and a zero initial condition, then sequentially running the other two models. Since the jump from one simulated mode to another is instantaneous, the test data fluctuate around steady-state values.

Fig. 5 gives scatter plots of the test data described above. As the data points in each case overlap, it is difficult to visually distinguish each mode from one another, particularly in the first case shown in Fig. 5(a).

In this paper, the number of autoregressive terms is determined using the Partial Autocorrelation Function (PACF) against a confidence bound of 5% [30]. For multivariate data, the calculation of PACF can be based on the summed squares of all measurements. In order to evaluate the MARSS models, the estimated and predefined state-space models are tested using step response and zero initial conditions without noise. The results of step responses are shown in Fig. 4. It can be observed that the step responses of the models estimated using the MARSS learning agree well with the equivalent responses obtained for the original state-space models.

It should be noted that the experiments in Section IV-B and IV-C are separate. In Section IV-B, the training, validation and test data from each of the models are used. In Section IV-C, training and validation data are only from model 2.1 and 2.2 while the test set consists of the data from model 2.1, 2.2 and 2.3.

B. Mode identification within known operating modes

Results of mode identification within known operating modes are demonstrated in this subsection. Fig. 6(a) shows the trend plot of test data obtained by sequentially changing the operating modes, with duration of 600 samples for each mode. The on-line monitoring indicator result is presented in Fig. 6(b). The posterior probability of each model conditional on the measurements is calculated by (10) and shown in Fig. 6(c). The results of using models 2.1, 2.2 and 2.3 in Fig. 7 and models 3.1, 3.2 and 3.3 in Fig. 8 are obtained following the same experiment operation.

Table. I presents the performance of mode identification for the described models. The Mode Identification Accuracy (MIA) and False Alarm Rate (FAR) metrics are:

$$\begin{aligned} \text{MIA} &= \frac{\text{num}_{j,\text{I}}}{\text{num}_{j,\text{S}} - \text{num}_{j,\text{A}}} \\ \text{FAR} &= \frac{\text{num}_{j,\text{A}}}{\text{num}_{j,\text{S}}} \end{aligned} \tag{23}$$

where only in (23), j denotes the model number (e.g. 1.1, 2.1), $\text{num}_{j,\text{A}}$, $\text{num}_{j,\text{I}}$ and $\text{num}_{j,\text{S}}$ are respectively the number of false alarms, the number of successfully identified samples and the number of samples from the model j. The results in Table I show that the FKF is capable of distinguishing data points derived from various dynamic and steady-state models.

C. Anomaly detection and mode identification when a new operating mode appears

This subsection demonstrates the monitoring performance for a process containing known operating modes and one new operating mode. Training and validation data were generated from state-space models 2.1 and 2.2 while the data to be classified were generated from models 2.1, 2.2 and 2.3. The FKF model only contains the dynamic and steady-state characteristics from models 2.1 and 2.2. Model 2.3 was treated as a new mode.

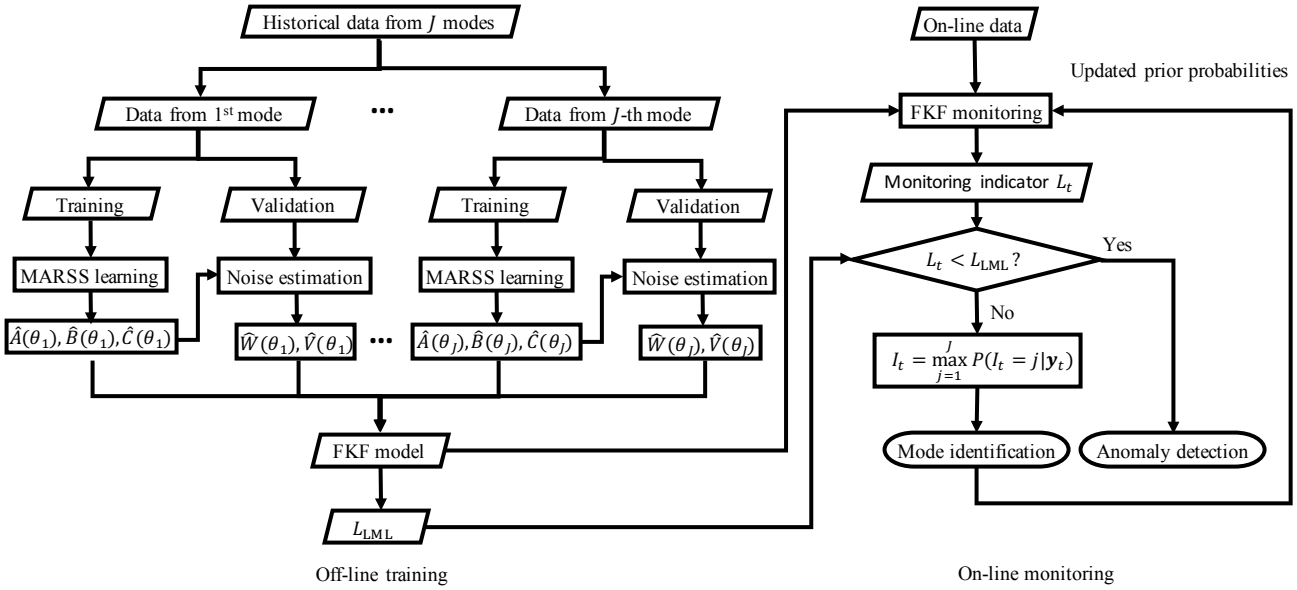

Fig. 3. Flowchart of off-line training the FKF monitoring model and on-line monitoring.

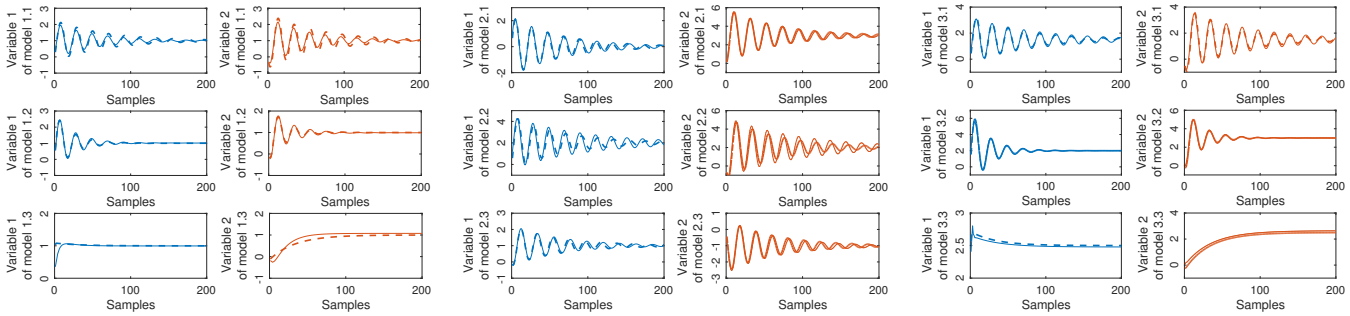

(a) Same steady-state, with three different dynamics

(b) Three different steady-states with the same dynamics

(c) Three different steady-states and three different dynamics

Fig. 4. Step response comparison between the MARSS models (solid lines) and simulated models (dashed lines).

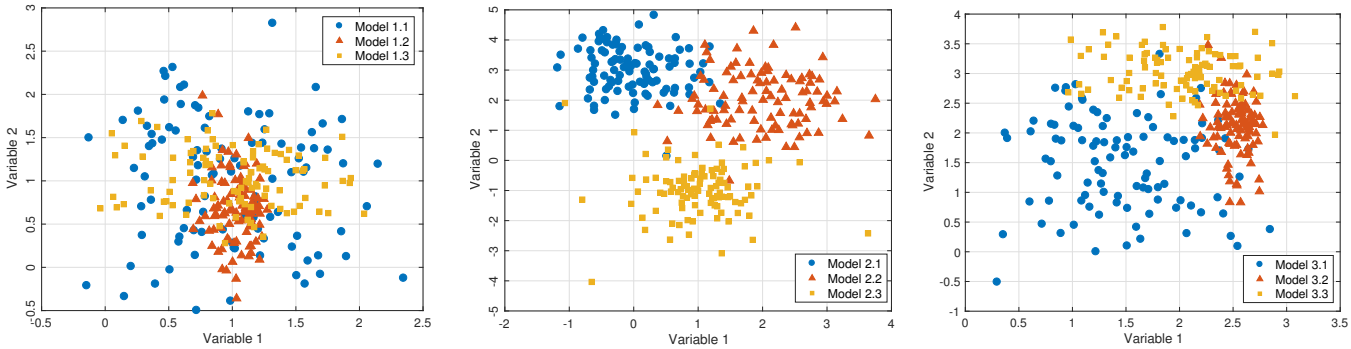

(a) Same steady-state, with three different dynamics

(b) Three different steady-states with the same dynamics

(c) Three different steady-states and three different dynamics

Fig. 5. Scatter plot for test data from models defined in Table V.

TABLE I
PERFORMANCE OF MODE IDENTIFICATION ON THREE MULTIMODE SIMULATION MODELS

Dynamic and steady-state models	Model number	$\text{num}_{j,\text{A}}$[a]	FAR [b]	$\text{num}_{j,\text{S}}$[c]– $\text{num}_{j,\text{A}}$	$\text{num}_{j,\text{I}}$[d]	MIA[e]
Same steady-state, with three different dynamics	Model 1.1	23	3.83%	577	499	86.48%
	Model 1.2	18	3.01%	581	562	96.90%
	Model 1.3	35	5.83%	565	557	98.58%
three different steady-states with the same dynamics	Model 2.1	26	4.33%	574	574	100%
	Model 2.2	30	5.01%	569	569	100%
	Model 2.3	37	6.17%	563	563	100%
three different steady-states and three different dynamics	Model 3.1	49	8.17%	551	551	100%
	Model 3.2	18	3.01%	573	573	98.79%
	Model 3.3	12	2.00%	588	588	100%

[a] The number of false alarms w.r.t. model j;
[b] False Alarm Rate;
[c] The number of samples from the model j;
[d] The number of successfully identified samples from model j;
[e] Mode Identification Accuracy;

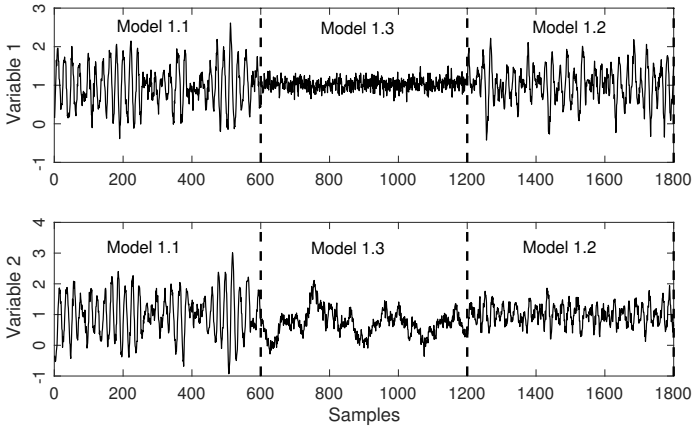

(a) Trend plot of samples

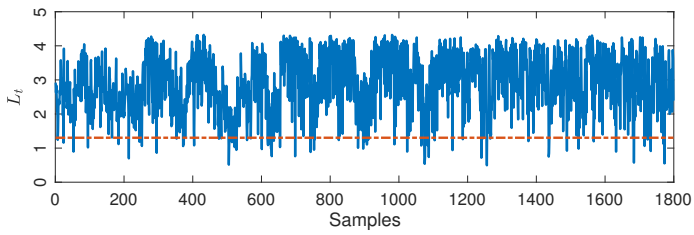

(b) On-line monitoring indicator. Blue-solid line is L_t; red-dashed line is L_{LML}.

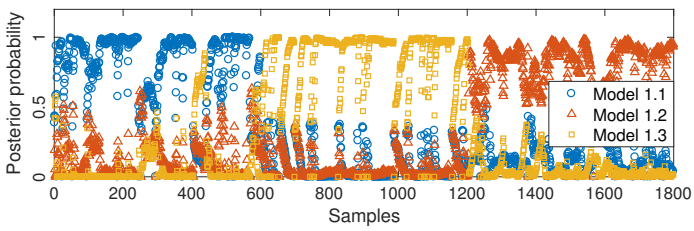

(c) On-line mode identification

Fig. 6. Monitoring results: the operation scheme is model 1.1, model 1.3 and model 1.2.

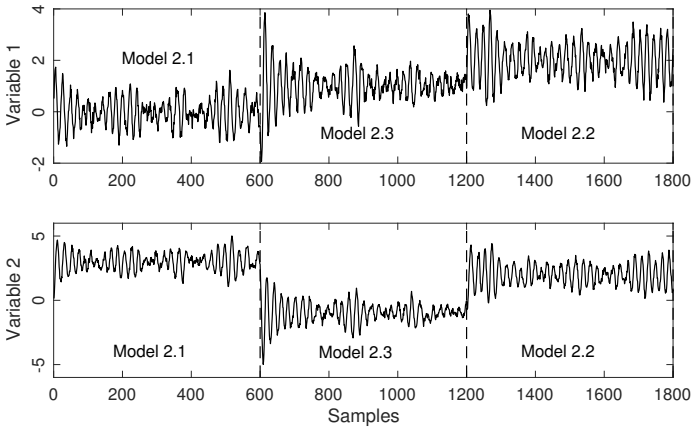

(a) Trend plot of samples.

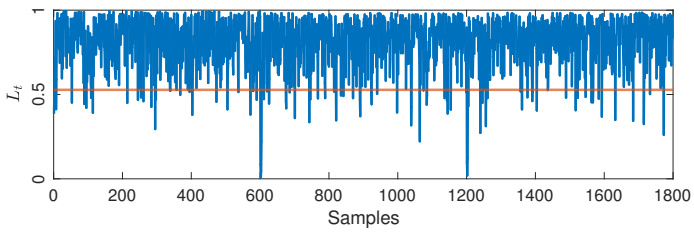

(b) On-line monitoring indicator. Blue-solid line is L_t; red-dashed line is L_{LML}.

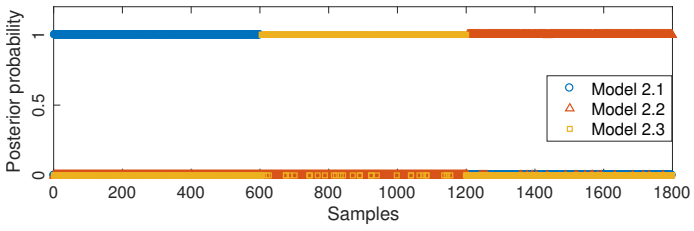

(c) On-line mode identification

Fig. 7. Monitoring results: the operation scheme is model 2.1, model 2.3 and model 2.2.

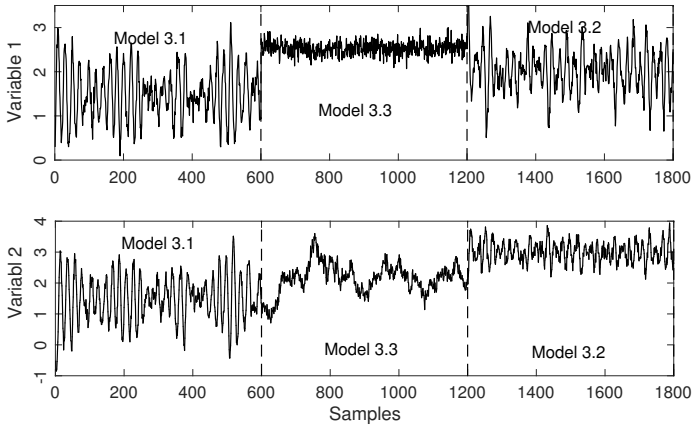

(a) Trend plot of samples.

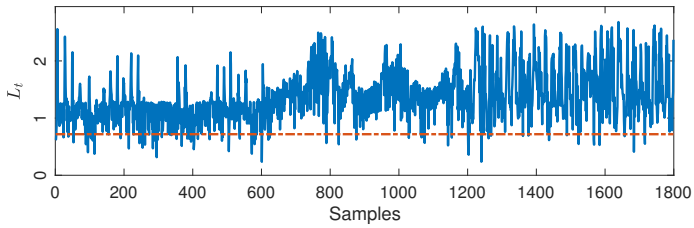

(b) On-line monitoring indicator. Blue-solid line is L_t; red-dashed line is L_{LML}.

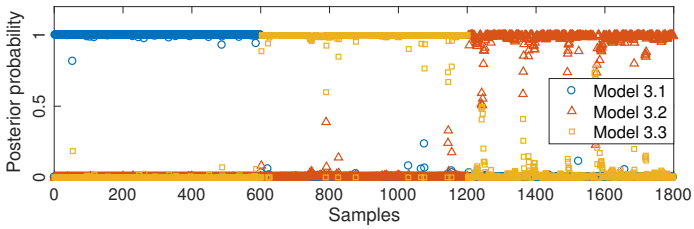

(c) On-line mode identification

Fig. 8. Monitoring results: the operation scheme is model 3.1, model 3.3 and model 3.2.

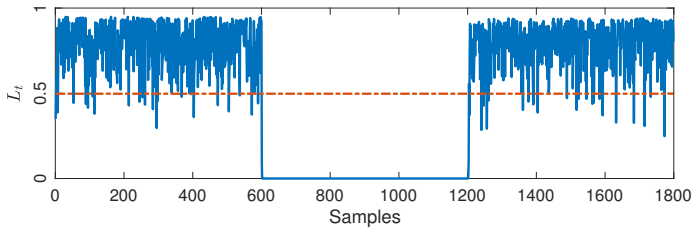

(a) On-line anomaly detection. Blue-solid line is L_t; red-dashed line is L_{LML}.

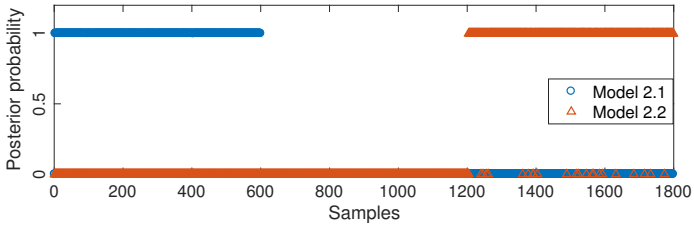

(b) On-line mode identification

Fig. 9. Anomaly detection and mode identification when a new operating mode appears.

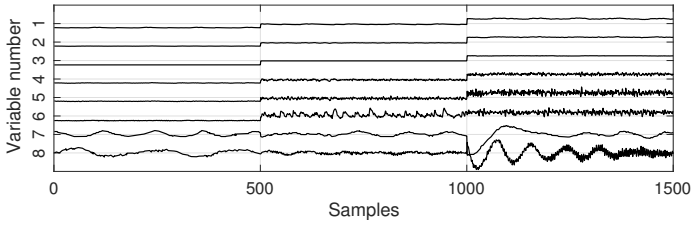

(a) Training data

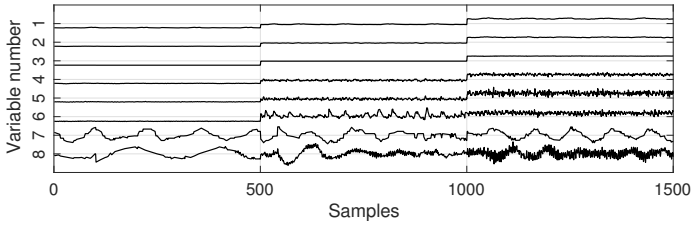

(b) Validation data

Fig. 10. Trend plots of training and validation data

Fig. 9 shows the monitoring results of test data including known operating modes and an additional mode. The on-line operating scheme is model 2.1, 2.3 and 2.2. Initially, the posterior probability and L_t indicate that the process was operating in the mode described by known model 2.1. It can be seen that L_t quickly responds to the occurrence of model 2.3, dropping down below the red-dashed line of L_{LML}, and posterior probabilities for model 2.1, 2.3 and 2.2 are 0. When model 2.2 occurs in the process, L_t returns to a level above L_{LML} and the maximal posterior belongs to model 2.2. The results show that the proposed monitoring indicator L_t is able to detect that the operating mode is unknown.

V. Industrial Case Study

This section demonstrates the effectiveness of anomaly detection and mode identification based on FKF using data recorded from an industrial scale multiphase flow facility. Specifically in this paper we utilise the PRONTO benchmark dataset [23].

A. Description of dataset

The PRONTO benchmark data were collected from a pilot-scale multiphase flow rig which allows the study of transportation, measurement and control of multiphase flows [23]. Various operating modes were implemented by adjusting the water and air flow rate. Reference [23] gives more details on the multiphase flow facility and the data.

The data used in this paper are from three normal operating mode datasets and one fault. Specific set points for normal operating modes are summarised in Table II. The air blockage fault was induced by gradually closing a valve in the inlet air line under Mode 1. There are eight variables are used for monitoring, presented in Table III.

After the data labelling step, the training dataset contains samples $1, 2, \ldots, 500$ from Mode 1, Mode 2 and Mode 3, and the validation dataset contains samples $501, 502, \ldots, 1000$ from Mode 1, Mode 2 and Mode 3. Fig. 10 highlights the

TABLE II
DETAILS OF NORMAL OPERATING MODES IN PRONTO BENCHMARK DATASET

Mode identity	Mode 1	Mode 2	Mode 3
Water flow rate (kg s^{-1})	0.1	0.5	1
Air flow rate (m^3 h^{-1})	120	150	200

TABLE III
LIST OF PROCESS VARIABLES IN PRONTO BENCHMARK DATASET

Variable Number	Variable description	umit
1	Input air flow rate	kg s^{-1}
2	Air delivery pressure	barg
3	Input water flow rate	kg m^3
4	Pressure in the mixing zone	barg
5	Pressure at the riser top	barg
6	2-phase separator output water flow rate	barg
7	3-phase separator pressure	barg
8	3-phase separator water level	%

TABLE IV
QUANTITATIVE COMPARISON AMONG FKF, FGMM-BIP AND PCA-BASED T^2 AND SPE

	FKF	FGMM-BIP	PCA
Classified training data?	✓	✓	✗
Mode identification	✓	✓	✗
Anomaly detection?	✓	✓	✓
Process models necessary?	✗[a]	✗	✗
Unified monitoring indicator?	✓	✓	✗
False alarm rate	2.67%	26.01%	T^2: 3.05% SPE: 0.53%
Anomaly detection time	3375	2394	T^2: 3907 SPE: 4457
Identification time of Mode 2	507	1190	N/A
Identification time of Mode 3	658	1185	N/A

[a] Incorporating an MARSS learning step in the proposed FKF removes the necessity of acquiring process model with first-principles;

trends of process variables in the training and validation dataset. The test dataset contains additional samples from Mode 1, Mode 2 and Mode 3, and all of the samples from the air blockage fault. The sequence of valve opening and the plot of test data are shown in Fig. 11(a) and 11(b).

B. Performance

In this demonstration, the FKF model for a multimode process in the dataset was derived from training data using the method in Section II-B. The performance of on-line anomaly detection and mode identification is presented in Fig. 11(c) and 11(d), respectively.

At time 0, since the FKF starts at artificially specified zero initial conditions different from the set points of the normal operating modes, it leads to a transient response in the L_t indicator. After the initial transient, the monitoring indicator goes above L_{LML} and the probabilistic outcomes in Fig. 11(c) indicate the current mode is Mode 1. Mode switches take place at sample 503 (A_1 in Fig. 11(d)) and 1185 (A_2 in Fig. 11(d)), causing a fast fall in monitoring indicators. After the FKF is adapted to the switched mode, the monitoring indicators return back to normal, and the maximal posterior probabilities correctly indicate periods where the process was operating in Mode 2 and Mode 3. The process variables have larger variances when the process runs at Mode 2 and Mode 3, relative to Mode 1, which can be seen in Fig. 11(b). Therefore, the monitoring indicator L_t varies over a wide range.

The valve closure fault (Fig. 11(a)) starts at sample 1312 (A_3 in Fig. 11(d)). The change from Mode 3 to a faulty operation is unlearned, resulting in L_t falling below the monitoring threshold. Then the monitoring indicator goes up, and initially, the operating mode continues to be recognised as Mode 1. This is likely because of a non-linear relationship existing between the valve adjustment and the associated flow changes. Adjustments to the valve cause only minor changes in flow regime until the valve is almost half closed, thus the incipient fault behaves similarly to Mode 1. At sample 2908 (A_4 in Fig. 11(d)), the monitoring indicator L_t shifts to a lower level, but does not trigger the monitoring threshold L_{LML}. When the valve opening degree decreases to 30 degrees, L_t at sample 3375 (A_5 in Fig. 11(d)) drops below L_{LML} accounting for the moderate fault. The posterior probability in Fig. 11(c) indicates an unknown mode once the fault is identified. As the fault becomes severe at sample 3900 (A_6 in Fig. 11(d)), L_t drops to a very small value, approaching to zero.

C. Comparison study

In this comparison study, process monitoring methods, FGMM-BIP index and PCA-based T^2 and SPE are compared against the FKF method. FGMM-BIP index [19] is a multimode process monitoring approach possessing both mode identification and anomaly detection abilities. In addition, FGMM-BIP index also uses the Bayesian inference technique and a unified monitoring indicator, similar to the FKF. PCA-based T^2 and SPE are extensively applied to detecting faulty operation in process industries [31].

1) Comparison with FGMM-BIP index : In [19], assuming the process data within each operating mode may be described by a multivariate Gaussian distribution, Finite Gaussian Mixture Models (FGMM) are used for determining the parameters (e.g. means, covariances and prior probabilities) associated with each operating mode. Further, a unified monitoring index, BIP, is defined by integrating Bayesian inference-based probability and distance-based probability.

In this comparison experiment, the code was implemented as described in [19]. The training data and test data are the same as the ones in Section V-A. Following [19], the monitoring limit was set to 95%. The fault is detected when the BIP index exceeds the monitoring limit. The mode identification and anomaly detection results using FGMM-BIP are presented in Fig. 12. Fig. 12(a) shows the on-line mode identification result. Similarly to the FKF monitoring method, the current operating mode is the one with the maximal posterior value.

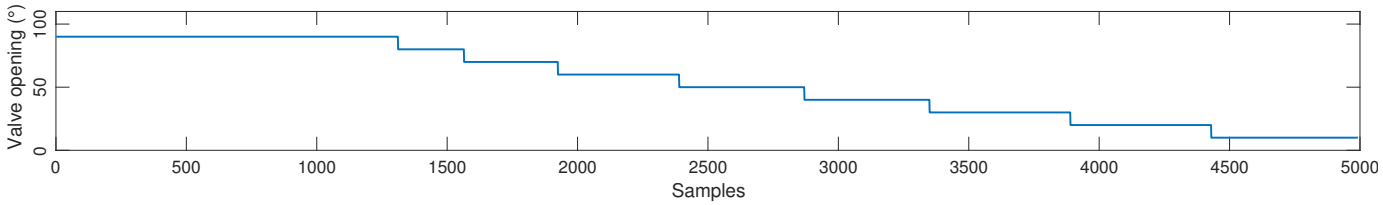

(a) The sequences of valve opening

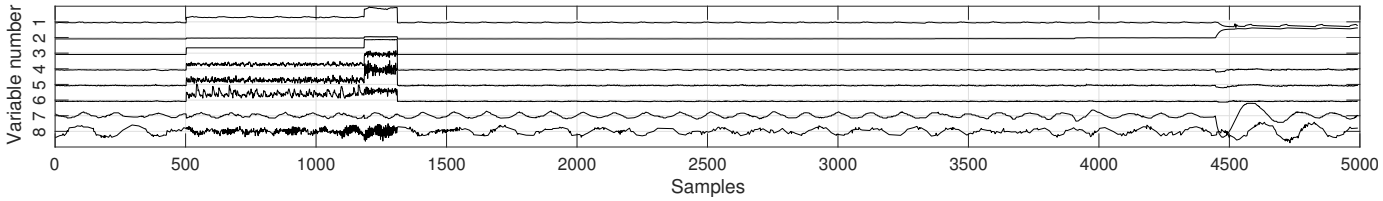

(b) Trend plot of test data

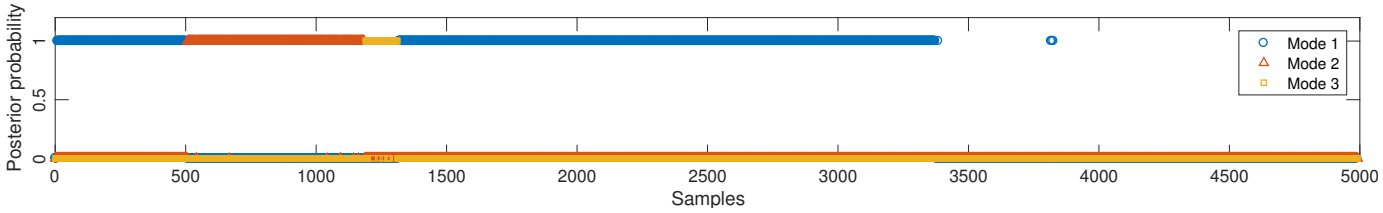

(c) On-line mode identification

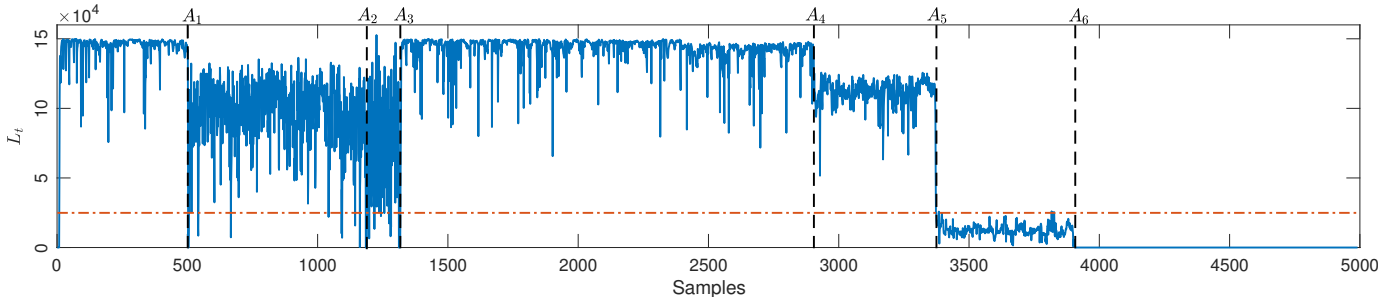

(d) On-line anomaly detection. The monitoring threshold L_{LML} is in the red dashed line. The solid line is the monitoring indicator L_t. A_1 and A_2: the action of mode switch. A_3: the appearance of fault. A_5: moderate fault. A_6: severe fault.

Fig. 11. FKF for anomaly detection and mode identification on PRONTO benchmark dataset

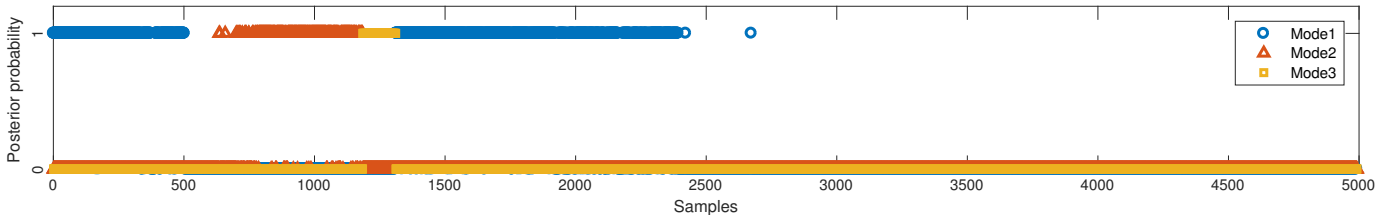

(a) On-line mode identification

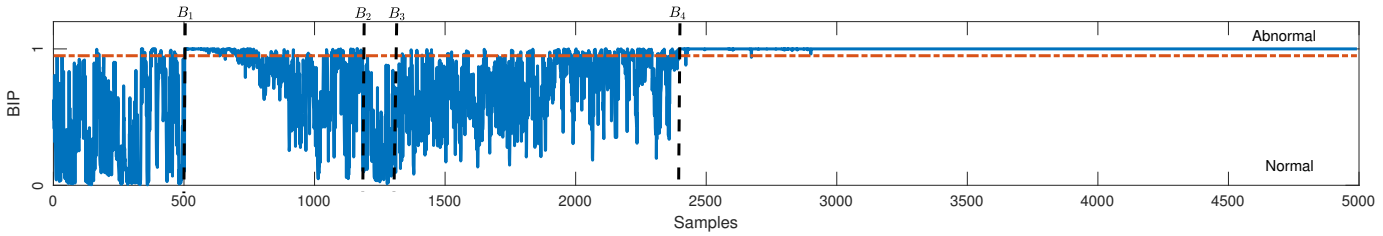

(b) On-line anomaly detection: the monitoring indicator BIP (the solid line) above the monitoring threshold (the dashed line) indicates that the process is at abnormal operation whereas at normal operation. B_1 and B_2: the action of mode switch. B_3: the appearance of fault. B_4: fault detection.

Fig. 12. FGMM-BIP for anomaly detection and mode identification on PRONTO benchmark dataset

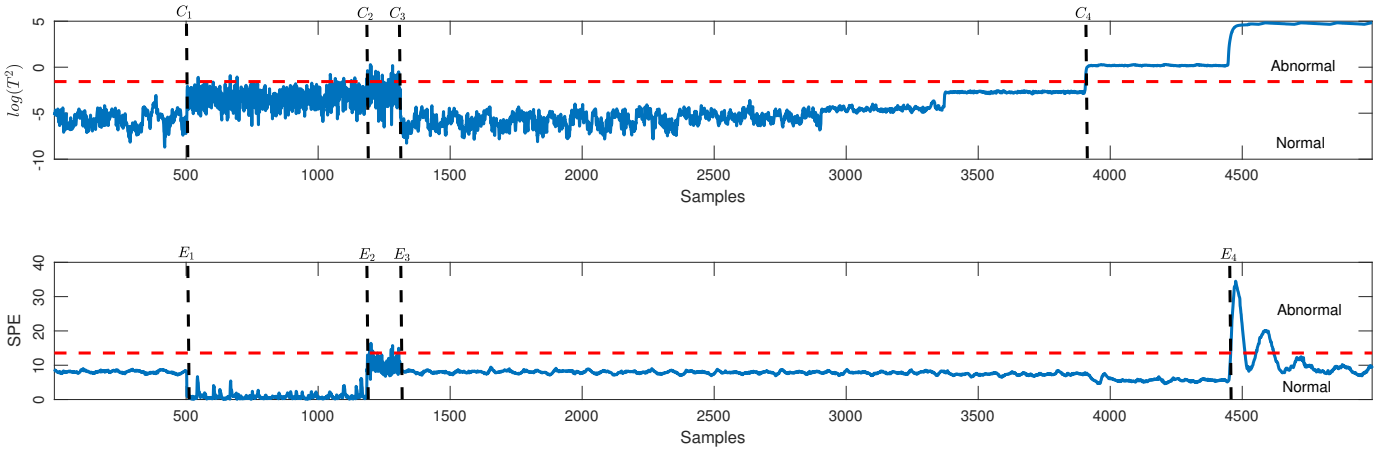

Fig. 13. PCA-based T^2 and SPE for anomaly detection on PRONTO benchmark dataset: the monitoring indicators T^2 and SPE (the solid lines) above the monitoring thresholds (the dashed line) indicates that the process is at abnormal operation whereas at normal operation. C_1/E_1 and C_2/E_2: the action of mode switch. C_3/E_3: the appearance of fault. C_4/E_4: fault detection.

The FGMM-BIP detects the the valve-opening anomaly just before sample 2394 (B_4 in Fig. 12(b)), 981 samples before the FKF method. On the other hand FGMM-BIP gives numerous false alarms during normal operation, and also gives false alarms after the mode change at sample 503 (B_1 in Fig. 12(b)).

The switch of mode at sample 503 (B_1 in Fig. 12(b)) is interpreted by FGMM-BIP as faulty operation. In addition, the BIP indicates anomalies until sample 658, even though the new mode is normal. The FKF method identified the switch of mode somewhat earlier at sample 507 and stopped indicating anomalies. Similarly to the FKF, the FGMM-BIP method identifies the period from sample 1312 (B_3 in Fig. 12(b)) to 2394 (B_4 in Fig. 12(b)) as normal operation in Mode 1. This is the period when the fault has started and is increasing in severity. Neither method is able to detect the fault in its early stages. Other studies using the same dataset, for example, [23], [32], also presented and discussed the difficulties in classifying and detecting this developing fault in early stages. These studies highlighted that the relationship between the valve position and flow rate is non-linear, and that there is only a minor change in the flow rate as the valve closes. Hence detection based on flow rate is delayed regardless of the detection algorithm.

When compared with the monitoring obtained using the FKF, the FGMM-BIP method shortens the delay of anomaly detection. Although the FGMM-BIP can detect the actual fault at an earlier stage than the FKF approach, the associated false alarm rate is significantly higher.

2) Comparison with PCA-based T^2 and SPE: The MATLAB code of computing T^2 monitoring statistic is from [33], while SPE statistic was implemented by authors based on [34]. Due to the fact that T^2 and SPE are not capable of mode identification, both were only applied to anomaly detection. Fig. 13 plots the monitoring results. T^2 detects the fault at sample 2907 (C_4 in Fig. 13) while SPE only detects the fault in a brief moment at sample 4457 (E_4 in Fig. 13).

The quantitative comparisons are conducted among three process monitoring methods, FKF, FGMM-BIP and PCA-based T^2 and SPE, respectively. The comparison results are given in Table IV.

VI. Conclusions

In order to systematically implement the FKF in the application of monitoring a multimode process, this paper presented a method of off-line training an FKF monitoring model and on-line anomaly detection and mode identification.

In this paper, the FKF model for a multimode process is a set of state-space models. Each state-space model is trained by MARSS learning and noise estimation using historical data. A universal monitoring indicator L_t is defined and a lower monitoring limit L_{LML} is trained off-line. The quality of the fit of the MARSS models and the performance of the FKF-based anomaly detection and mode identification are tested on simulated multimode processes. The results presented in Section IV show that the the MARSS models trained using historical data are capable of reflecting the dynamic and steady-state characteristics and therefore are applicable for model-based anomaly detection and mode identification. Particularly, the case of same steady state, with three different dynamics show that the FKF is sensitive to the dynamics, thereby showing it is able to perform a mode identification task for dynamic models. Experiments using data recorded from an industrial scale multiphase flow facility confirmed that the proposed workflow in Section III may also be applied in practical settings. In addition, the comparison results in Section V-C show that the proposed unified monitoring indicator is able to detect anomalies while resulting in fewer false alarms.

The performance of anomaly detection relies on the sensitivity of the FKF monitoring model. If the FKF model is trained using data that are not fully representative of normal operation, the resulting model will not be accurate. As a result, the FKF monitoring model will be less sensitive to the occurrences of faulty operation.

Appendix

For the simulation case, the training and validation datasets and test data to be classified are derived using the state-space

TABLE V
MATRIX SPECIFICATION FOR STATE-SPACE MODELS.

Dynamic and steady-state model combinations	Model number	Matrix A	Matrix B	Matrix C	steady-states
(1) Models with same steady- states and different dynamics	Model 1.1	$\begin{bmatrix} 0.9267 & -0.2183 \\ 0.3882 & 0.9558 \end{bmatrix}$	$\begin{bmatrix} 0.2917 \\ -0.3440 \end{bmatrix}$	$\begin{bmatrix} 1 & 0 \\ 0 & 1 \end{bmatrix}$	$\begin{bmatrix} 1 \\ 1 \end{bmatrix}$
	Model 1.2	$\begin{bmatrix} 0.8791 & -0.4239 \\ 0.1884 & 0.9566 \end{bmatrix}$	$\begin{bmatrix} 0.5521 \\ -0.1451 \end{bmatrix}$	$\begin{bmatrix} 1 & 0 \\ 0 & 1 \end{bmatrix}$	
	Model 1.3	$\begin{bmatrix} 0.0418 & -0.0703 \\ 0.1250 & 0.9796 \end{bmatrix}$	$\begin{bmatrix} 1.0285 \\ -0.1047 \end{bmatrix}$	$\begin{bmatrix} 1 & 0 \\ 0 & 1 \end{bmatrix}$	
(2) Models with different steady-states and same dynamics	Model 2.1	$\begin{bmatrix} 0.9267 & -0.2183 \\ 0.3882 & 0.9558 \end{bmatrix}$	$\begin{bmatrix} 0.6550 \\ 0.1327 \end{bmatrix}$	$\begin{bmatrix} 1 & 0 \\ 0 & 1 \end{bmatrix}$	$\begin{bmatrix} 0 \\ 3 \end{bmatrix}$
	Model 2.2	$\begin{bmatrix} 0.9267 & -0.2183 \\ 0.3882 & 0.9558 \end{bmatrix}$	$\begin{bmatrix} 0.5834 \\ -0.6879 \end{bmatrix}$	$\begin{bmatrix} 1 & 0 \\ 0 & 1 \end{bmatrix}$	$\begin{bmatrix} 2 \\ 2 \end{bmatrix}$
	Model 2.3	$\begin{bmatrix} 0.9267 & -0.2183 \\ 0.3882 & 0.9558 \end{bmatrix}$	$\begin{bmatrix} -0.1450 \\ -0.4324 \end{bmatrix}$	$\begin{bmatrix} 1 & 0 \\ 0 & 1 \end{bmatrix}$	$\begin{bmatrix} 1 \\ -1 \end{bmatrix}$
(3) Models with different steady-states and different dynamics	Model 3.1	$\begin{bmatrix} 0.9267 & -0.2183 \\ 0.3882 & 0.9558 \end{bmatrix}$	$\begin{bmatrix} 0.4375 \\ -0.5159 \end{bmatrix}$	$\begin{bmatrix} 1 & 0 \\ 0 & 1 \end{bmatrix}$	$\begin{bmatrix} 1.5 \\ 1.5 \end{bmatrix}$
	Model 3.2	$\begin{bmatrix} 0.8791 & -0.4239 \\ 0.1884 & 0.9566 \end{bmatrix}$	$\begin{bmatrix} 1.5280 \\ -0.2468 \end{bmatrix}$	$\begin{bmatrix} 1 & 0 \\ 0 & 1 \end{bmatrix}$	$\begin{bmatrix} 2 \\ 3 \end{bmatrix}$
	Model 3.3	$\begin{bmatrix} 0.0418 & -0.0703 \\ 0.1250 & 0.9796 \end{bmatrix}$	$\begin{bmatrix} 2.5712 \\ -0.2616 \end{bmatrix}$	$\begin{bmatrix} 1 & 0 \\ 0 & 1 \end{bmatrix}$	$\begin{bmatrix} 2.5 \\ 2.5 \end{bmatrix}$

models in Table V. These models are predefined to give a range of under-damped and over-damped transient dynamics.

ACKNOWLEDGMENT

This work was supported by the European Union's Horizon 2020 research and innovation programme under grant agreement No. 675215 - PRONTO - H2020-MSCA-ITN-2015.

REFERENCES

[1] Z. Yu and J. Falnes, "State-space modelling of a vertical cylinder in heave," *Applied Ocean Research*, vol. 17, pp. 265–275, 1995.

[2] D. Hinrichsen and A. Pritchard, *Mathematical Systems Theory I: Modelling, State Space Analysis, Stability and Robustness*. Berlin: Springer-Verlag, 2005.

[3] S. Tan, F. Wang, J. Peng, Y.Q. Chang, and S. Wang, "Multimode process monitoring based on mode identification," *Industrial & Engineering Chemistry Research*, vol. 51, pp. 374–388, 2012.

[4] A. Akca, and E. M Önder, "Multiple model Kalman and Particle filters and applications: a survey," *IFAC-PapersOnLine*, vol. 52, no. 3 pp. 73–78, 2019.

[5] T. Kobayashi and D. L. Simon, "Evaluation of an enhanced bank of Kalman filters for in-flight aircraft engine sensor fault diagnostics," *Journal of Engineering for Gas Turbines and Power*, vol. 127, pp. 497–504, 2005.

[6] W. Xue, Y. Guo, and X. Khorasani, "A bank of Kalman filters and a robust Kalman filter applied in fault diagnosis of aircraft engine sensor/actuator," *International Conference on Innovation Computing*, 2007.

[7] N. Meskin, E. Naderi, and K. Khorasani, "Bank of Kalman filters for fault detection in quad rotor MAV," *ARPN Journal of Engineering and Applied Sciences*, vol. 11, no. 10, pp. 6668–6674, 2016.

[8] R. Chen, X. Wang, and J. Liu, "Adaptive joint detection and decoding in flat-fading channels via mixture Kalman filtering," *IEEE Transactions on Information Theory*, vol. 46, no. 6, pp. 2079–2094, September 2000.

[9] S. Huang, K. Tan, and T. Lee, "Fault diagnosis and fault-tolerant control in linear drives using the Kalman filter," *IEEE Transactions on Industrial Electronics*, vol. 59, no. 11, pp. 4284–4292, 2012.

[10] J. Alkahe, Y. Oshman, and O. Rand, "Adaptive estimation methodology for helicopter blade structural damage detection," *Journal of Guidance, Control, and Dynamics*, vol. 25, no. 6, pp. 1049–1057, 2002.

[11] N. Meskin, E. Naderi, and K. Khorasani, "A multiple model-based approach for fault diagnosis of jet engines," *IEEE Transactions on Control Systems Technology*, vol. 21, no. 1, pp. 254–262, 2013.

[12] P. Bania and J. Baranowski, "Field Kalman filter and its approximation," *2016 IEEE 55th Conference on Decision and Control (CDC)*, pp. 2875–2880, 2016.

[13] J. Baranowski, P. Bania, I. Prasad, and T. Cong, "Bayesian fault detection and isolation using field Kalman filter," *EURASIP Journal on Advances in Signal Processing*, vol. 79, no. 1, 2017.

[14] R. Frigola, F. Lindsten, T. Schön, and C. Rasmussen, "Bayesian inference and learning in Gaussian process state-space models with particle MCMC," *Advances in Neural Information Processing Systems 26*, pp. 3156–3164, 2013.

[15] R. Frigola and C. Rasmussen, "Integrated preprocessing for Bayesian nonlinear system identification with Gaussian processes," *52th Annual Conference on Decision and Control*, pp. 5371–5376, 2013.

[16] W. Larimore, "Canonical variate analysis in identification, filtering and adaptive control," *29th IEEE Conference on Decision and Control*, pp. 596–604, 1990.

[17] E. Holmes, E. Ward, and K. Wills, "MARSS: Multivariate autoregressive state-space models for analyzing time-series data," *the R Journal*, vol. 4, pp. 11–19, 2012.

[18] H. Akaike, "Fitting autoregressive models for prediction," *Annals of the Institute of Statistical Mathematics*, vol. 21, pp. 243–247, 1969.

[19] J. Yu and S.J. Qin, "Multimode process monitoring with Bayesian inference-based finite Gaussian mixture models," *AIChE Journal*, vol. 54, no. 7, pp. 1811–1829, 2008.

[20] H. White, "Consequences and detection of misspecified nonlinear regression models," *Journal of the American Statistical Association*, vol. 76, no. 374, pp. 419–433, 1981.

[21] X. Song, M. Wu, C. Jermaine, and S. Ranka, "Conditional anomaly detection," *IEEE Transactions on Knowledge and Data Engineering*, vol. 19, no. 5, pp. 631–645, May 2007.

[22] Z. Ge and Z. Song, "Mixture Bayesian regularization method of PPCA for multimode process monitoring," *American Institute of Chemical Engineers (AlChE) Journal*, vol. 56, no. 11, pp. 2838–2849, 2010.

[23] A. Stief, R. Tan, Y. Cao, J.R. Ottewill, N.F. Thornhill, and J. Baranowski, "A heterogeneous benchmark dataset for data analytics: multiphase flow facility case study," *Journal of Process Control*, vol. 79, pp. 41–55, 2019.

[24] K. Zhang, K. Peng, and J. Dong, "A common and individual feature extraction-based multimode process monitoring method with application to the finishing mill process," *IEEE Transactions on Industrial Informatics*, vol. 14, pp. 4841–4850, November 2018.

[25] I. Ben-Gal, "Outlier detection," in *Data mining and knowledge discovery handbook*, O. Maimon, L. Rokach, Ed. Springer, 2005, pp. 131–146.
[26] R. Tan, T. Cong, J.R. Ottewill, J. Baranowski and N.F. Thornhill, "An on-line framework for monitoring nonlinear processes with multiple operating modes," *Journal of Process Control*, vol. 89, pp. 119–130, 2020.
[27] S. Weisberg, *Applied Linear Regression*. John Wiley and Sons, 1980.
[28] N.F. Thornhill, M. Oettiger, and P. Fedenczuk, "Refinery-wide control loop performance assessment," *Journal of Process Control*, vol. 9, no. 109-124, 1999.
[29] P. Maybeck, "Multiple model adaptive algorithm for detecting and compensating sensor and actuator/surface failures in aircraft flight control systems," *International Journal of Robust and Nonlinear Control*, vol. 9, pp. 1051–1070, 1999.
[30] A. R. and R. Agrawal, "An introductory study on time series modelling and forecasting," *Lamber Academic Publishing: Saarbrücken*, 2013.
[31] K.E. Pilario, M. Shafiee, Y. Cao, L.Y. Lao and S.H. Yang, "A Review of Kernel Methods for Feature Extraction in Nonlinear Process Monitoring," *Processes*, vol. 8, no. 1, pp.24, 2020.
[32] R. Tan, J.R. Ottewill and N.F. Thornhill, "Nonstationary Discrete Convolution Kernel for Multimodal Process Monitoring," *IEEE Transactions on Neural Networks and Learning Systems*, pp.1–12, 2019.
[33] K.E. Pilario, "PCA-based Fault Detection for 2D Multivariate Process Data," https://www.mathworks.com/matlabcentral/fileexchange/65983-pca-based-fault-detection-for-2d-multivariate-process-data, MATLAB Central File Exchange. Retrieved May 14, 2020.
[34] C. Ruiz-Cárcel, Y. Cao and D. Mba, L. Lao and R.T. Samuel, "Statistical process monitoring of a multiphase flow facility," *Control Engineering Practice*, vol. 42, pp.74–88, 2015.

Tian Cong received the B. Eng. degree from the University of Shanghai for Science and Technology, China, in 2014, and the M. Eng. degree from the Australian National University, Australia, in 2016. Currently, she is studying towards the Ph.D. degree at AGH University of Science and Technology, Kraków, Poland.

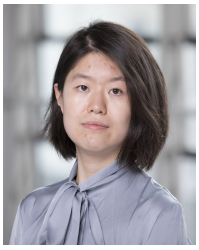

Ruomu Tan received the B.Eng. degree from Zhejiang University, China, in 2013 and the M.Sc. degree from the University of Alberta, Canada, in 2015. She is currently working towards the Ph.D. degree at Imperial College London, London, U.K. Meanwhile, she is a research scientist at ABB Corporate Research Center in Ladenburg, Germany. Her research interests include data-driven nonlinear process monitoring, multivariate statistical analysis and their application to process industries.

James R. Ottewill was born in London, U.K. He received the B.Eng. degree (with honors) in mechanical engineering from the University of Bristol, Bristol, UK in 2005 and the Ph.D. degree in mechanical engineering from the same university in 2009. He is currently a Senior Principal Scientist at Hitachi ABB Power Grids Research in Kraków, Poland working in the field of applied analytics for condition monitoring applications. His main research interests relate to advanced physics-based and data-driven approaches for diagnostics and prognostics including dynamic testing, modeling and analysis of non-linear systems, signal processing and information fusion. Dr. Ottewill is a Chartered Engineer in the U.K. and a Member of the Institution of Mechanical Engineers, U.K.

Nina F. Thornhill (SM'93) received the B.A. degree in physics from Oxford University, Oxford, U.K., in 1976, the M.Sc. degree from Imperial College London, London, U.K., and the Ph.D. degree from University College London. She is a Professor in the Department of Chemical Engineering at Imperial College London where she holds the ABB Chair of Process Automation.

Jerzy Baranowski (M'11) was born in Kraków, Poland. He received the master's, D.Phil., and D.Sc. degrees in automatic control and robotics from the AGH University of Science and Technology, Kraków, Poland, in 2006, 2010, and 2017, respectively. He is currently an Associate Professor with the Department of Automatic Control and Robotics, AGH University of Science and Technology and leads its laboratory of Computer Science in Control and Management. His current research interests include fault detection, Bayesian statistics, and applications of fractional calculus. Dr. Baranowski is an Academic Editor for the Mathematical Problems in Engineering. He was the recipient of the scholarship of Polish Ministry of Science and Higher Education for outstanding young scientists in 2017.